J. Fluid Mech. (1981), *vol.* 105, *pp.* 119–142
Printed in Great Britain

Dynamics of an impinging jet. Part 1. The feedback phenomenon

By CHIH-MING HO AND NAGY S. NOSSEIR†
Department of Aerospace Engineering, University of Southern California, Los Angeles

(Received 27 March 1980 and in revised form 1 July 1980)

In a high-speed subsonic jet impinging on a flat plate, the surface pressure fluctuations have a broad spectrum due to the turbulent nature of the high-Reynolds-number jet. However, these pressure fluctuations dramatically change their pattern into almost periodic waves, if the plate is placed close to the nozzle ($x_0/d < 7{\cdot}5$). In the present study extensive measurements of the near-field pressure provide solid support for the hypothesis that a feedback mechanism is responsible for the sudden change observed in the pressure fluctuations at the onset of resonance. The feedback loop consists of two elements: the downstream-convected coherent structures and upstream-propagating pressure waves generated by the impingement of the coherent structures on the plate. The upstream-propagating waves and the coherent structures are phase-locked at the nozzle exit. The upstream-propagating waves excite the thin shear layer near the nozzle lip and produce periodic coherent structures. The period is determined by the convection speed of the coherent structures, the speed of the upstream-propagating waves as well as the distance between the nozzle and the plate. An instability process, herein referred to as the 'collective interaction', was found to be critical in closing the feedback loop near the nozzle lip.

1. Introduction

The impinging jet can be viewed as a synthesis of a number of diverse flow modules, namely a free turbulent jet, stretched vortices in a curved shear layer, a stagnation flow, and a wall jet, with each portion of the flow having its own distinctive characteristics. These features have attracted much fundamental research into the impinging-jet configuration. The impinging jet is also important in many technological developments. For example, on some STOL aircraft the high-speed exhaust from the jet engine is deflected by direct impingement on the flaps to create extra lift during take-off. Fatigue due to excessive dynamic loading on the flaps and high levels of noise radiation are among problems encountered in such designs. When the jet is operated at high subsonic speeds ($M > 0{\cdot}7$) and the nozzle-to-plate distance is of the order of the potential core length or less ($x_0/d < 7{\cdot}5$), the fluctuating pressure becomes an almost-periodic wave-form (see figure 2 below). The spectra normalized to their r.m.s. pressure fluctuations (figure 3) show that the energy increases in a relatively narrow frequency

† Present address: Department of Applied Science, New York University, 26–36 Stuyvesant St, New York, N.Y. 10003.

band, the resonance frequency, while it diminishes at all other frequencies. The dynamic loading on the surface exhibits a much stronger spatial coherence and is as much as 50% higher than the loading in a non-resonant jet (Ho & Nosseir 1980). Therefore the resonance not only poses an interesting topic for basic research but it also has important practical applications.

An extensive study of the impinging jet was carried out by Donaldson, Snedeker & Margolis (1971) in order to understand the heat transfer near the stagnation region. Velocity profiles and pressure distributions were carefully documented for a wide range of parametric variations. Gutmark, Wolfshtein & Wygnanski (1978) investigated a plane jet impinging on a flat plate located 100 slot-widths downstream. They found that the flow properties on the centre-plane of the jet are essentially the same as in a free jet except in a short region (about 20% of the distance between the slot and the plate) in front of the solid boundary. Their spectral measurements detected a frequency range in which turbulent energy is neither augmented nor attenuated. At higher frequencies the turbulence is attenuated owing to viscous dissipation, while at lower frequencies the turbulence is augmented presumably because of vortex stretching as the fluid approaches the plate. Foss & Kleis (1976) studied shallow-angle ($< 12°$) impingement. Their measurements suggest that a finite-length stagnation line, instead of a stagnation point, exists on the plate. The surface pressure fluctuations on curved plates impinged upon by an axisymmetric jet were measured by Ho, Plocher & Leve (1977). The general characteristics of the fluctuating pressure, such as the normalized maximum fluctuation level, the peak frequency and the roll-off exponent of the spectra, do not change with the geometry of the plate. Only the streamwise distribution of the r.m.s. pressure fluctuations is affected by the curvature of the solid boundary.

It is known that a broad class of flows exhibit similar self-sustained oscillations (Rockwell & Naudascher 1979). The edgetone, flow over a cavity, and an impinging jet all belong to the same category. A common characteristic of these flows is a free shear flow impinging on a solid boundary. A pressure disturbance produced by the impinging flow structures is fed back to force the inherently unstable free shear layer. This feedback loop generates the self-sustained oscillation and the screech tone. For the edgetone problem, Powell (1961) modelled the feedback from the edge as a dipole source and established a value of unity for the 'gain around the circuit' as the criterion for self-sustained oscillation. Many features of the edgetone phenomenon can be explained by his formulation. In the case of an impinging jet, Wagner (1971) reported that the self-sustained oscillations occur at $M > 0{\cdot}6$ and $x_0/d < 6$. Visualization by schlieren photography was used to examine the flow field. Based upon the standing-wave pattern inside the jet, he suggested that a feedback of pressure waves through the jet core was responsible for the resonance. Neuwerth (1973) obtained the resonant frequency by measuring the far-field noise. The frequencies vary with distance from the solid boundary and form several stages, which is a characteristic feature in many flows with self-sustained oscillations. Neuwerth, following the same argument as Wagner based his model on acoustic feedback from within the jet core. Unfortunately no reliable measurements can be made inside a high-speed jet. The present study indicates that the resonance phenomenon can be understood from near-field measurements taken outside the jet column. Furthermore, Nosseir (1979) used a theoretical approach similar to Ribner's (1957) to calculate the induced transverse

velocity by forcing in a shear layer. The results show that a thin shear layer is more susceptible to upstream acoustic forcing from outside the jet than from within.

The movies taken by Neuwerth (1973) demonstrated the importance of the coherent structures. An understanding of the role of the coherent structures in an impinging shear layer is necessary for studying the resonant jet. The idea of large-scale structures in a turbulent flow was first introduced by Townsend (1956), but extensive study on this subject did not start until Brown & Roshko (1971) reported their work. They recognized that the structures not only have scales comparable to the thickness of the shear layer but also are coherent in the lateral direction. The technique of conditional sampling reported by Kovasznay, Kibens & Blackwelder (1970) facilitated the experimental study of coherent structures in various shear flows. In a circular jet, Lau, Fisher & Fuchs (1972) found that the coherent structures travel at a speed equal to 60 % of the jet exit velocity. They also measured the phase relationship between the pressure fluctuations and the velocity components. The results agree with a simple model using a vortex array to represent the shear layer. Browand & Laufer (1975) reported that the Strouhal number of the passing structures at the end of the potential core is close to 0·5 and is independent of the Reynolds number.

The present study of the resonant impinging jet provides a solid experimental support for the feedback mechanism which has been proposed by theoreticians (for example, Powell 1961; Tam & Block 1978) in similar flows with self-sustained oscillations. First, two branches of the feedback loop, the downstream-convected coherent structures and the upstream-propagating waves, are established. The characteristics of the upstream-propagation waves are determined. Then, the phase relationship between the coherent structures and the upstream-propagation waves at the plate and the nozzle exit is identified. Finally, a phenomenon named 'collective interaction' is observed and shown to be an essential mechanism for self-sustained oscillations.

It is worth mentioning here that near-field microphones were used to measure the pressure induced by the passing turbulent eddies. In order to follow more closely the measured quantity, i.e. the induced pressure, the term 'downstream-travelling waves' is used to represent the convected turbulent eddies throughout the text.

2. Facility and data processing

2.1. *Facility*

The air jet (figure 1) consisted of a stagnation chamber and a 2·54 cm diameter nozzle with a contraction ratio of 289:1. The turbulence level in the stagnation chamber was measured and found to be 0·4 %. The stagnation pressure was regulated by a low-noise control valve. The variation of the stagnation pressure during the measurements was maintained to within 2 % of the mean gauge pressure. Five large storage tanks allow the jet to be operated for a time from 3 min to 10 min, depending on the Mach number and the size of nozzle. The jet exit Mach number was restricted to the subsonic range 0·3 to 0·9 in the present experiment. The jet is located in an anechoic chamber with dimensions 4·78 m wide by 6·20 m long by 3·63 m high. The low-frequency cut-off of the chamber is 150 Hz.

A flat steel plate (76·20 × 76·20 × 0·64 cm) was used to provide a large surface for the impinging jet. The plate was mounted on a traverse mechanism with 4 degrees of freedom with the streamwise and transverse movements remotely controlled. The

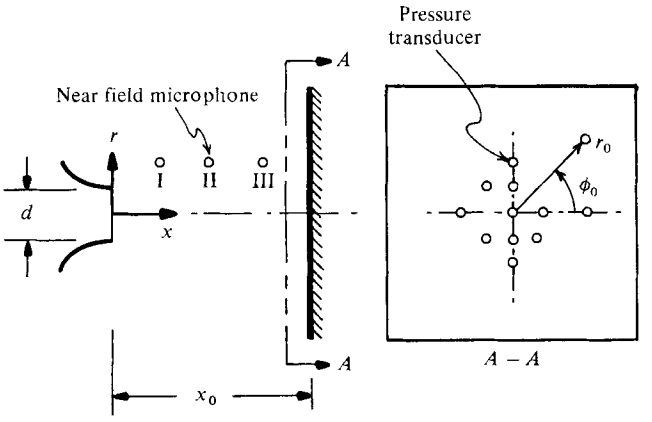

FIGURE 1. Schematic diagram of the impinging jet.

plate and its supporting mechanism were examined for structural vibrations during jet operation. The vibrations of the plate were measured with an accelerometer (Bruel and Kjaer type 4324). At $M = 0{\cdot}9$ the amplitude of vibrations was only $2{\cdot}84 \times 10^{-5}$ cm.

The surface pressure fluctuations were measured by 0·32 cm diameter Kulite XTEL-1-190-25 piezoresistive pressure transducers with natural frequency in excess of 100 kHz. There were 46 transducer sites on the plate and the unused sites were filled by flush-mounted plugs. Measurements of pressure fluctuations in the region between the nozzle and the plate were made in the hydrodynamic near field of the jet, using 0·32 cm ($\frac{1}{8}$ inch) diameter Bruel and Kjaer type 4138 condenser microphones with frequency response from 7 Hz to 140 kHz.

The cylindrical co-ordinate system is defined in figure 1. The streamwise direction is x, the radial direction and the azimuthal direction are r and ϕ respectively. The diameter of the jet d and the acoustic wavelength at the resonant frequency $\lambda_a = a/f_r$ (a is the ambient speed of sound) are used as length scales for normalization. The subscript 0 denotes the co-ordinates on the plate. Functions with Arabic numerals as subscripts (for example correlation function $R_{2,3}$) represent measurements associated with surface pressure transducers. Functions with Roman numerals as subscripts (for example, $R_{\mathrm{II,III}}$) represent data associated with near-field microphones.

2.2. *Data processing*

All the signal outputs were recorded on a Hewlett–Packard 14-channel tape recorder (Type 3955A). For FM mode recording, the frequency response is from d.c. to 20 kHz. For direct mode recording, the frequency band is from 300 Hz to 300 kHz. The analog data are digitized and processed by a PDP 11/55 minicomputer. The fast Fourier transform (FFT) technique is used for all the spectral analysis.

When the jet is in resonance the pressure signals have the form of slightly distorted sine waves (figure 2). The spectra then are dominated by a peak at the resonant frequency, while the correlation functions would show a sinusoidal behaviour with no distinguishable optimum peak. A data-processing method called pre-whitening is quite useful for analysing small random signals superimposed on a high-amplitude

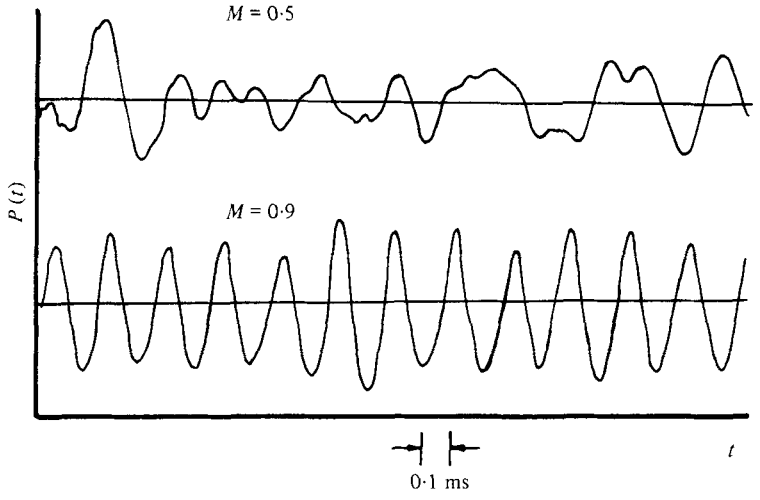

FIGURE 2. Signals of surface pressure fluctuations ($x_0/d = 4$, $r_0/d = 0$). The case $M = 0{\cdot}5$ is an example of non-resonance; the case $M = 0{\cdot}9$ is an example of resonance.

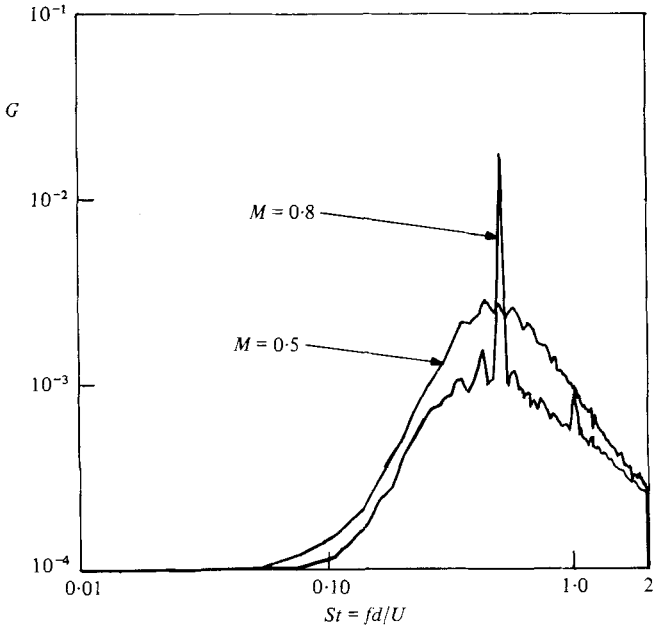

FIGURE 3. Normalized power spectra of surface pressure fluctuations ($x_0/d = 4$, $r_0/d = 1{\cdot}5$). The curve $M = 0{\cdot}8$ corresponds to resonance.

pure tone. A conventional pre-whitening technique (Williams & Purdy 1970) separates the random signals from the pure tone by subtracting an in-phase sine wave from the original signal by analog methods. A pre-whitening technique was developed (Nosseir 1979) using digital methods, and was found to be much simpler. The procedure to obtain the pre-whitened cross-correlation function of two signals was to replace the

high resonant peak in the cross-spectrum with the averaged value of the two neighbouring frequency components, and then to inverse-Fourier transform the resulting spectrum. After removing the two peaks at the resonant frequency and its first harmonic, the pre-whitened correlation does exhibit a distinctive optimum peak. The delay time of this peak will be used to calculate a broad-band eddy convection velocity.

3. Experimental results

3.1. *The two branches of the feedback loop*

It has been suggested for some time (Powell 1961) that two wave trains, one travelling downstream and one travelling upstream, form a feedback loop and should be phase-locked at the nozzle lip in order to close the loop. Although knowledge of the characteristics of the upstream-propagating waves is necessary in clarifying important links in the feedback loop, most experiments have only studied the downstream-travelling waves in detail. The first step in the present experiment is to establish the existence of the two branches of the feedback loop.

The pre-whitening technique can be used to identify the directions of wave propagation. The correlation between two microphones I and II in the near field of the jet is shown in figure 4(*a*). The correlation $R_{\mathrm{I,II}}(\tau)$ is a sine wave as one would expect from two resonant signals and does not provide any clues about the propagation directions of the waves. However, two peaks at positive and negative time delays (figure 4*b*) of the pre-whitened correlation $\tilde{R}_{\mathrm{I,II}}(\tau)$ do suggest the possibility of two waves propagating in opposite directions. When the two microphones were moved farther away from the jet axis ($r/\lambda_a > 1{\cdot}0$), the correlation showed only the negative time delay peak (figure 5), indicating the dominance of the upstream-travelling waves there. These promising results provide opportunities to investigate the feedback loop through near-field pressure measurements.

(*a*) *Characteristics of the upstream-propagating waves.* The pressure signals, from which figure 5 was produced, came from microphones placed within one acoustic wavelength λ_a of the jet axis, which was still inside the hydrodynamic near field. Data indicates the dominance of the upstream-travelling waves in this region. In an effort to understand the characteristics of the upstream-propagating waves, the phase speed and the direction of wavefront propagation were examined through two-point statistics. From two microphones placed at fixed points in the near field one can determine an apparent phase speed either from the correlation function or from the cross-spectrum. In order to obtain the true phase speed, more information about the wavefront had to be obtained. Hence measurements taken at more than two points were necessary.

The wavefront was mapped from a pair of microphones; one is fixed near the nozzle lip (at $r/d = 0{\cdot}51$) and the other placed at several different stations in a plane perpendicular to the jet axis at $x = 0$. The phase differences between the two signals at the resonance frequency, $\nu(f_r)$, are obtained from the phase spectra and are plotted in figure 6 for different probe separations. Away from the jet axis ($r/\lambda_a > 1{\cdot}0$), the phase difference increases almost linearly with the radial distance. In this region, the upstream-travelling waves appear to be dominant from the pre-whitened correlation curve (figure 5). Therefore, the upstream-travelling waves have almost conical wave fronts for $r/\lambda_a > 1{\cdot}0$. The direction of propagation of the wavefront is determined

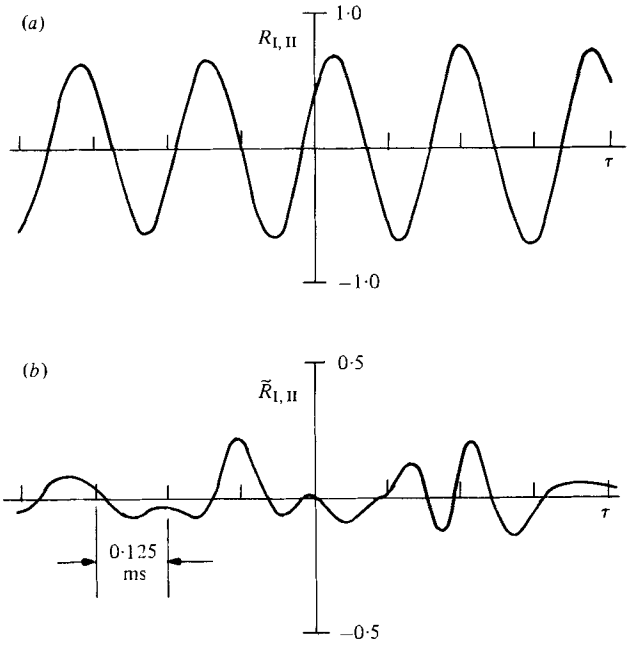

FIGURE 4. Cross-correlation of near-field pressure signals, (*a*) before prewhitening, (*b*) after prewhitening ($M = 0{\cdot}9$, $x_0/d = 5$). For microphone I, $x/d = 0{\cdot}10$, $r/d = 0{\cdot}52$; for microphone II, $x/d = 1{\cdot}95$, $r/d = 0{\cdot}93$.

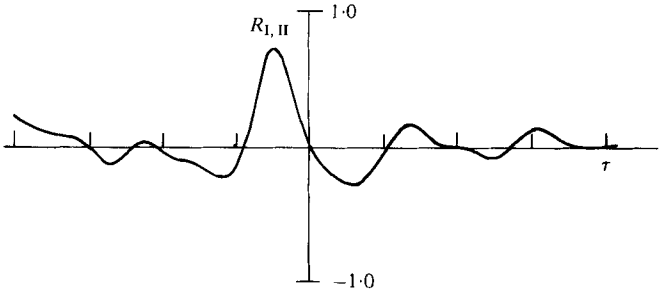

FIGURE 5. Cross-correlation of near-field pressure signals away from the jet axis ($M = 0{\cdot}9$, $x_0/d = 5$). For microphone I, $x/d = 0{\cdot}10$, $r/d = 2{\cdot}7$; for microphone II, $x/d = 1{\cdot}02$, $r/d = 2{\cdot}7$.

from the rate of change of phase angle with respect to the radial distance according to the following relation:

$$\theta_a = \sin^{-1}\left[\frac{1}{2\pi}\frac{d\nu(f_r)}{d(r/\lambda_a)}\right], \tag{1}$$

where θ_a is the angle between the jet axis and the unit vector perpendicular to the wavefront. For a nearly conical wavefront, an averaged value of θ_a is

$$\overline{\theta}_a = \sin^{-1}\left[\frac{1}{2\pi}\frac{\overline{d\nu(f_r)}}{d(r/\lambda_a)}\right]. \tag{2}$$

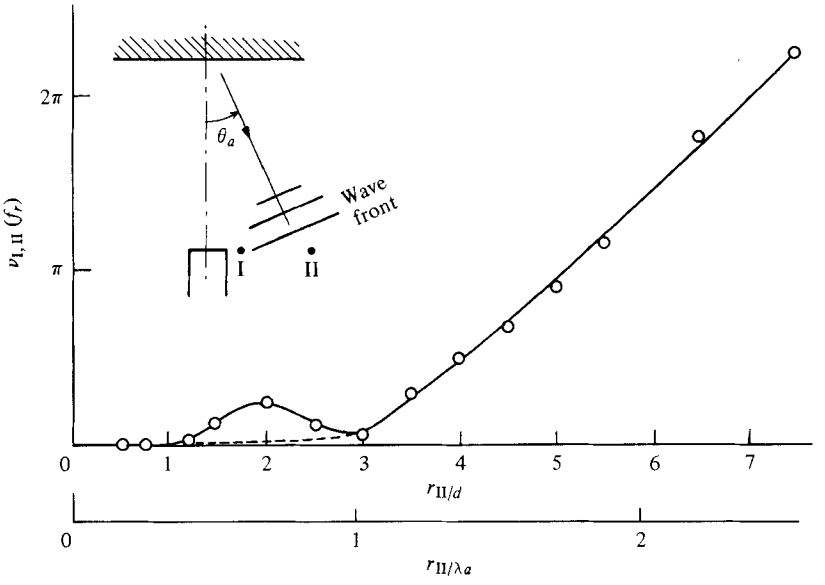

FIGURE 6. Variation of the phase angle at the resonant frequency near the nozzle exit ($M = 0{\cdot}9$, $x_0/d = 5$). For microphone I, $x/d = 0{\cdot}1$, $r/d = 0{\cdot}51$; for microphone II, $x/d = 0{\cdot}1$.

For the nozzle-to-plate distance, $x_0/d = 5$, the values of $\bar{\theta}_a$ is 32·5°. The phase angle function (figure 6) has a small bulge near $r/\lambda_a = 0{\cdot}7$. The accuracy of measurement of the phase angle is poor near that region. The authors believe the phase angle distribution should follow the dashed line on the diagram.

The apparent phase velocity was measured using two microphones separated in the streamwise direction (see figure 7*b*). The upstream microphone was placed at several different distances in the radial direction. The phase angle $\nu_{III,II}(f)$ was calculated and three samples of the measurements are plotted in figure 7*a*. Since the output of microphone III was delayed, the positive slope indicates upstream-propagating waves. The phase angle increases linearly with the frequency, so the phase velocity is constant at all frequencies and the waves are non-dispersive. One also notices that deviations of $\nu_{III,II}(f)$ around its mean decrease as r_{II}/d increases due to the decay of the contamination from the downstream-travelling waves. The apparent phase velocity $\mathbf{C}_2'(f)$ is

$$\mathbf{C}_2'(f) = 2\pi\boldsymbol{\xi}_{III,II}\Big/\frac{\nu_{III,II}(f)}{f}, \tag{3}$$

where $\boldsymbol{\xi}_{III,II}$ is the vector joining microphones III and II. Since $\boldsymbol{\xi}_{III,II}$ does not necessarily coincide with the direction of wave propagation, the true phase velocity $\mathbf{C}_2(f)$ is

$$\mathbf{C}_2(f) = 2\pi\frac{(\boldsymbol{\xi}_{III,II}\cdot\boldsymbol{\theta}_a)}{\nu_{III,II}(f)/f}\boldsymbol{\theta}_a, \tag{4}$$

where $\boldsymbol{\theta}_a$ is the unit vector making an angle θ_a with the jet axis. Equation (4) is used to calculate the speed of the upstream-travelling wave. The magnitude of $\mathbf{C}_2(f)$ normalized to the ambient sonic speed a for different r_{II}/d is plotted in figure 7(*b*). The data

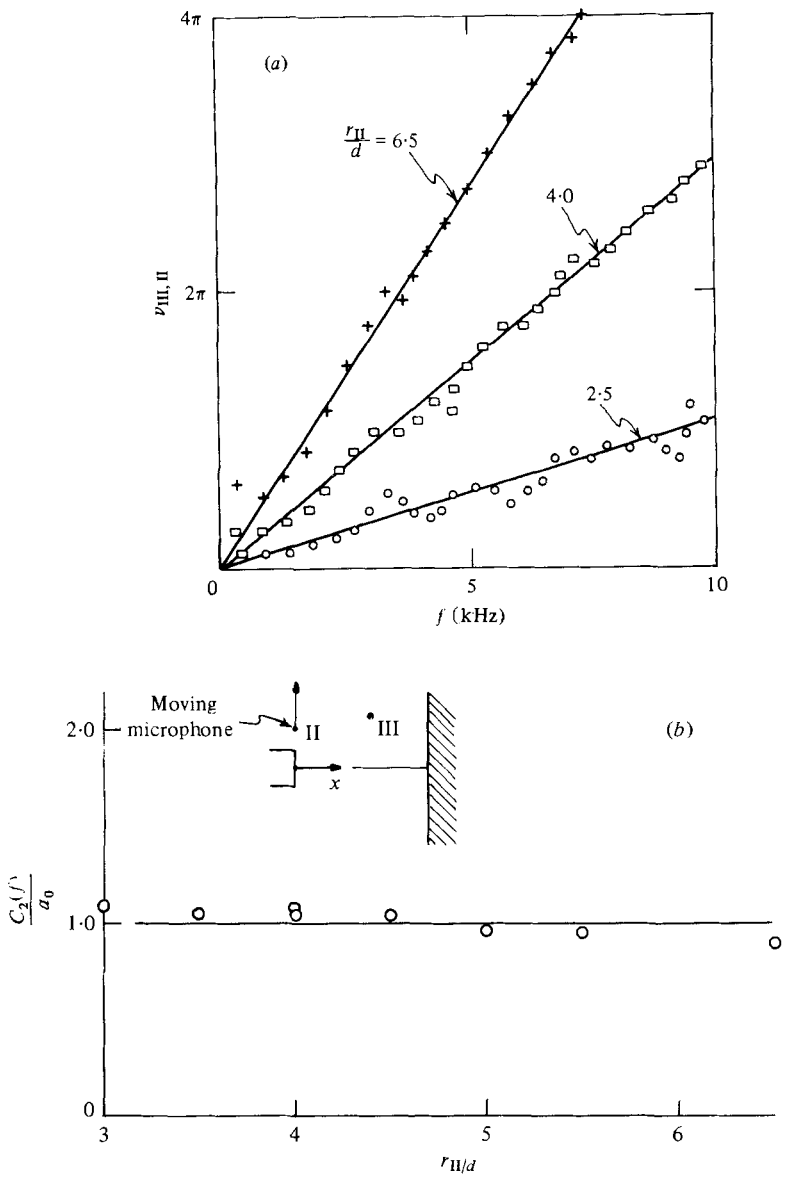

FIGURE 7. (*a*) Phase angle of near-field pressure signals near the nozzle (M = 0·9, x_0/d = 5). (*b*) Comparison between measured upstream-propagating wave velocity in the θ_a direction and plane acoustic waves (M = 0·9, x_0/d = 5, θ_a = 35°).

show, not surprisingly, that the waves travel at speeds close to the ambient speed of sound. A constant value of $\theta_a = 32{\cdot}5°$ was used in calculating $C_2(f)$ in figure 7(*b*). However, figure 6 shows that the slope is not really constant but increases slightly with increasing r/λ_a for $r/\lambda_a > 1{\cdot}0$. This results in smaller values of $C_2(f)/a_0$ for larger r_{II}/d, which indeed is the trend one observes in figure 7(*b*).

The two microphones separated in the streamwise direction can also be used to determine the direction of the wavefront propagation. When microphone II was

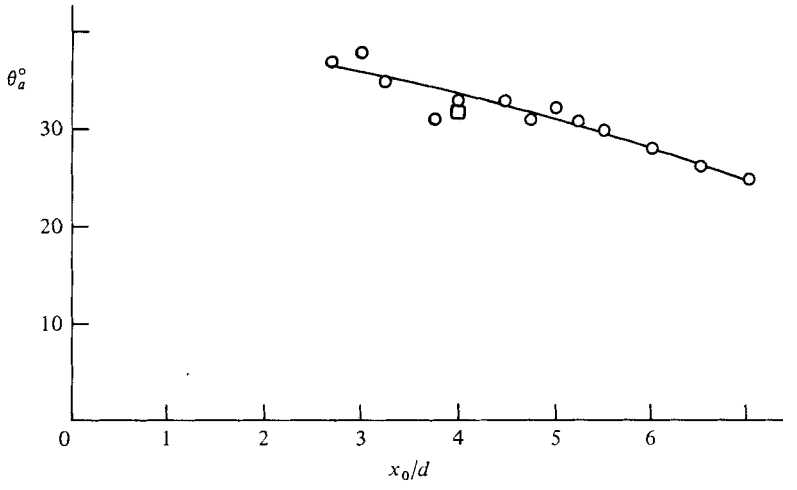

FIGURE 8. Measured angle between the upstream-propagating waves and the jet axis for different plate locations. □, $M = 0{\cdot}8$; ○, $M = 0{\cdot}9$.

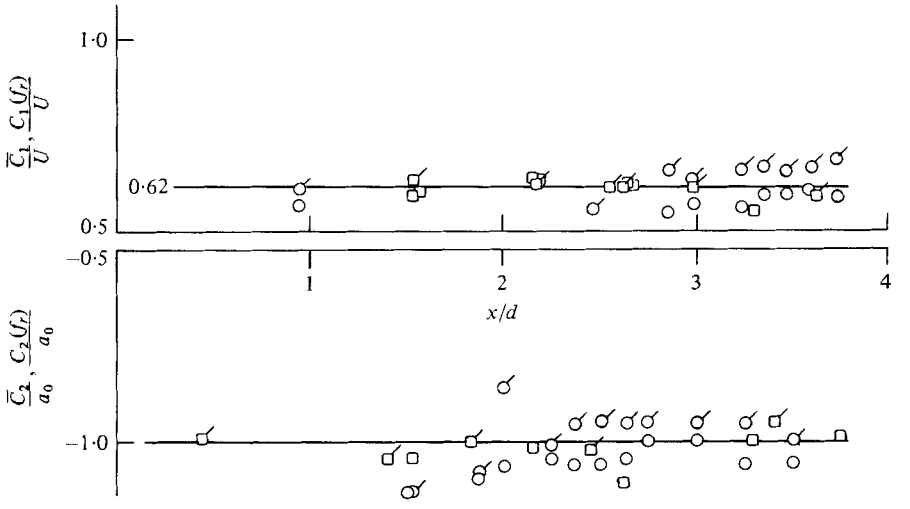

FIGURE 9. Propagation velocities of the downstream and the upstream waves: broadband velocity $\bar{C}_1$, $\bar{C}_2$ and phase velocity at the resonant frequency $C_1(f_r)$, $C_2(f_r)$. The straight line at $\bar{C}_1/U = 0{\cdot}62$ follows Neuwerth (1973).

moved in the radial direction, cross-correlations were calculated for each separation distance. The curve connecting the peaks of these correlations had a maximum at $r_{11}/d = 3{\cdot}5$ (Nosseir 1979). The relative position between the two microphones at this maximum gives the direction of wavefront propagation. This direction agrees with that determined from the phase measurements of figure 6. The direction of wavefront propagation varies with the positions of the plate (figure 8). The refraction effect by the wall jet on the upstream-travelling waves near the plate can account for the angle of propagation and its variation with nozzle-to-plate distance. The average wall jet

speed is about 50 % of the jet exit speed. Since the upstream-travelling wave propagates at sonic speed, the resultant angle of the wavefront is of the order of 30°. The average wall jet speed decreases with increasing nozzle-to-plate distance; so does the angle of propagation. The above results indicate that the upstream-propagating waves are travelling at sonic speed and inclined about 30° to the jet axis. The measured phase speeds in the direction $\boldsymbol{\theta}_a$ calculated either from the phase differences or from the cross-correlation are summarized in figure 9.

(*b*) *Characteristics of the downstream-travelling waves.* The wave speed of the downstream-travelling waves can be measured either from pre-whitened correlations $\bar{C}_1$, or from the phase difference at a certain frequency between two probes $C_1(f)$. The phase speeds at the resonance frequency $C_1(f_r)$ and the values of $\bar{C}_1$ are normalized to the jet exit speed U. The normalized values were found to be 0·62 (figure 9), which have been identified as the convection speed of the large coherent structures in a low-speed jet through hot-wire measurements (Lau *et al.* 1972) and in high-speed jet using frame-by-frame analysis of movies (Neuwerth 1973). The phase speed at the resonance frequency $C_1(f_r)$ being the same as the convection speed of the coherent structures indicates that the large coherent structures play the main role in the feedback mechanism.

(*c*) *A simple model of the near-field pressure waves.* If the autocorrelation of a near-field pressure waves is calculated, two extra peaks (denoted [3] and [4] in figure 10) appear at long time delays; they are symmetric with respect to zero time delay. These extra peaks also appear in the cross-correlations, but they are not symmetric with respect to zero time delay (figure 11). A very simple model proposed here satisfactorily explains these peaks.

The model (see appendix) assumes that the pressure at any point in the near field is a superposition of two plane waves: a wave travelling downstream at $C_1 = 0{\cdot}62U$ and a wave propagating upstream with the speed of sound in a direction making an angle θ_a to the jet axis. Since the upstream-propagating waves are generated by the impingement of the coherent structures, the phase difference between the two waves on the plate is zero. The calculated cross-correlation $R_{i,j}(\tau)$ of the fluctuating pressures at two locations, x_i and x_j, would exhibit four peaks with the following time delays:

$$\tau^{[1]} = (x_j - x_i)/C_1, \quad \tau^{[2]} = -\boldsymbol{\xi}_{i,j}.\boldsymbol{\theta}_a/C_2, \tag{5a,b}$$

$$\tau^{[3]} = -\left(\frac{x_0 - x_j}{C_1} + \frac{\boldsymbol{\xi}_{i,s}.\boldsymbol{\theta}_a}{C_2}\right), \quad \tau^{[4]} = \left(\frac{x_0 - x_i}{C_1} + \frac{\boldsymbol{\xi}_{j,s}.\boldsymbol{\theta}_a}{C_2}\right), \tag{5c,d}$$

where $\boldsymbol{\xi}_{i,s}$ and $\boldsymbol{\xi}_{s,j}$ are the vectors connecting x_i and x_j to an apparent sound source s on the plate in a region where the large-scale structures presumably impinge on the plate (Ho & Nosseir 1980). The interpretation of these time delays is as follows: $\tau^{[1]}$ is the time it takes the waves to travel downstream from x_i to x_j. $\tau^{[2]}$ is the time needed for the upstream waves to travel from x_j to x_i and should therefore appear as a negative time delay in $R_{i,j}(\tau)$. $\tau^{[3]}$ is the time required for the waves to travel downstream from x_j to the apparent source on the plate plus the time for the waves generated by the impingement to travel from the plate to x_i. $\tau^{[4]}$ is the time for the waves to travel from x_i to the plate at a speed of C_1 plus the time to travel from the apparent source to x_j with a speed C_2.

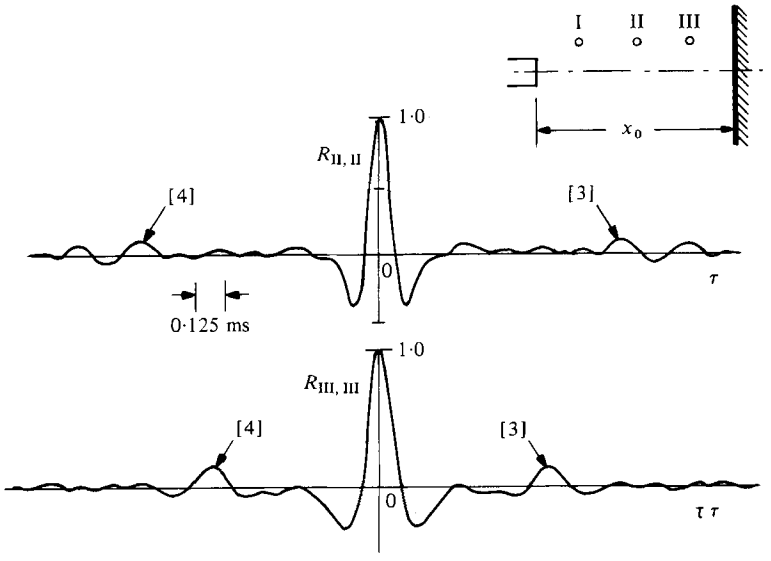

FIGURE 10. Autocorrelations of near-field pressure signals ($M = 0{\cdot}8$, $x_0/d = 7$). For microphone I, $x/d = 1{\cdot}09, r/d = 1{\cdot}13$; for II, $x/d = 1{\cdot}97, r/d = 1{\cdot}13$; for III, $x/d = 3{\cdot}25, r/d = 1{\cdot}31$.

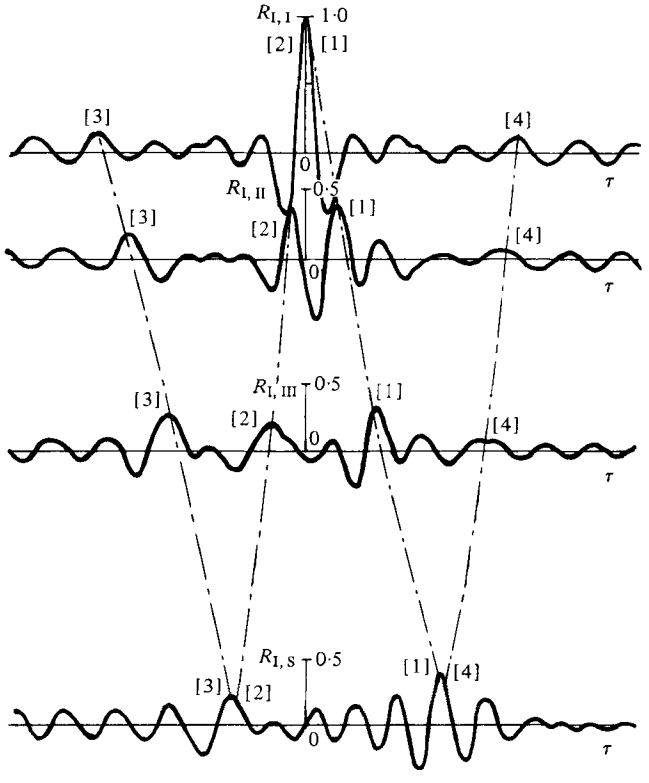

FIGURE 11. Correlations of near-field pressure signals; ($M = 0{\cdot}8$, $x_0/d = 5{\cdot}5$, $r_s/d = 1$) indices refer to the sketch in figure 10.

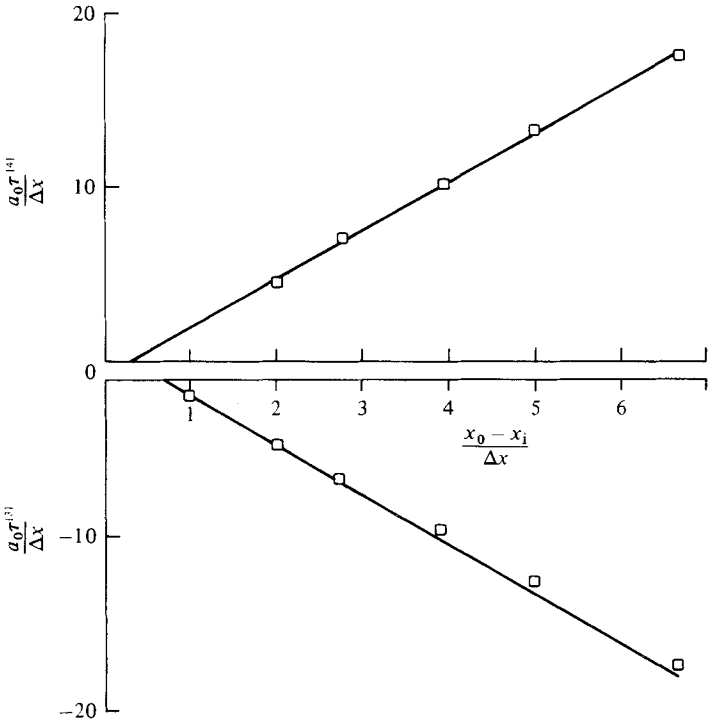

FIGURE 12. Time delays of peaks (3) and (4) in the correlations between near-field microphones separated by $\Delta x = x_j - x_i$, □, measured; ——, equation (5), $M = 0{\cdot}8$.

For the case of $x_i = x_j$, the autocorrelation function $R_{i,i}(\tau)$ has peaks with time delays given by

$$\tau^{[1]} = \tau^{[2]} = 0, \tag{6a}$$

$$\tau^{[4]} = \tau^{[3]} = \frac{x_0 - x_i}{C_1} + \frac{\boldsymbol{\xi}_{i,s} \cdot \boldsymbol{\theta}_a}{C_2}. \tag{6b}$$

Therefore, the extra peaks in the autocorrelation (figure 9) represent the time for waves to travel downstream from x_i to the plate and to return back from the plate to x_i.

The autocorrelation and cross-correlation of the signals from several pressure transducers placed along the streamwise direction are plotted in figure 11. The vertical spacing of the correlation curves in the diagram are scaled to the streamwise distances between each microphone. Lines connecting all the peaks form a W-shaped curve which indicates agreement between the model's predictions and the experimental values. A more precise comparison is made in figure 12. The calculated values of $\tau^{[3]}$ and $\tau^{[4]}$ are plotted against the measured data. The agreement is excellent. The success of this simple model can be attributed to the following fact. The correlation peaks appear at relatively long time delays and have long temporal coherence; therefore, they are mostly determined by pressure waves generated by the coherent structures which have low frequencies and long wavelengths. The complicated high-frequency small-scale turbulence has no major contributions to these peaks.

3.2. *The phase lock*

A wave travelling downstream and a wave propagating upstream in the near field have been detected. The mechanism of interaction between these waves at the nozzle exit remains to be clarified. The mechanism, to be described, serves to close the feedback loop for the observed self-sustained oscillations. Since the thin shear layer at the nozzle exit is intrinsically unstable, it is suggested that these self-excited oscillations are forced by the upstream-propagating waves with a sufficiently large amplitude that a phase lock is established at a fixed resonant frequency or frequencies. Experimental results are prescribed in this section to verify this contention.

The variations of the phase difference at the resonant frequency, $\nu(f_r)$, along the jet axis for both waves are presented in figure 13. The $\nu(f_r)$ variations from the nozzle lip to the plate along the downstream-travelling waves are presented by the upper curve. These phase angles are measured from the cross-spectra by a series of transducers placed along the outer edge of the shear layer. The lower curve represents $\nu(f_r)$ variations of the upstream-propagating waves from the plate back to the nozzle exit and were measured with microphones placed farther away from the shear layer ($r/d > 2{\cdot}5$). The reference point on the plate is at $r_0/d = 1$. This is a position in the region where large-scale structures were observed to impinge on the plate (Neuwerth 1973).

The slope of the upper curve in figure 13 is proportional to the inverse of the convection speed of the coherent structures. The slope of the lower curve represents the inverse of the sonic speed with a proportionality constant. At any streamwise position x/d, the difference between the two curves represents the phase difference between the two waves. The most important observation is that the phase difference at the nozzle exit ($x/d = 0$) is an integer multiple of 2π. This result has been confirmed for different nozzle-to-plate distances (Nosseir 1979). Therefore, the downstream-travelling waves must be locked in phase with the upstream-propagating waves at the nozzle exit.

When the impinging jet is operated in the resonant condition the resonant Strouhal number $(St)_r = f_r d/U$ varies with plate location for a fixed Mach number (figure 14*a*). The resonant Strouhal number decreases with increasing x_0/d until it reaches a minimum value of 0·3. For farther separation of the plate, the Strouhal number changes abruptly to a higher value, then decreases again with increasing nozzle-to-plate distances and the cycle repeats. These frequency stages are typical of flows with self-sustained oscillations such as flow over cavities and edgetones (Rockwell & Naudascher 1979).

The presence of the frequency stages becomes clear if one stipulates that resonance requires an integer number of waves N to exist in the feedback loop. By definition

$$N = \frac{x_0}{\lambda_1(f_r)} + \frac{x_0}{\lambda_2(f_r)}, \tag{7a}$$

where $\lambda_1(f_r) = C_1(f_r)/f_r$ and $\lambda_2(f_r) = [C_2(f_r)/\cos\theta_a]/f_r$ are the wavelengths of the downstream- and the upstream-travelling waves respectively. Equation (7*a*) characterizes the most fundamental feature of flows with a feedback loop.

The measured resonant frequencies are plotted according to equation (7*a*) in figure 14 (*b*). In each of the frequency stages, the number of waves, N, remains constant. As the nozzle-to-plate distance increases, the wavelength of both waves increases to preserve the phase lock at the nozzle exit. This results in a decrease in the resonant frequency. As the nozzle-to-plate distance is increased, the resonant frequency is

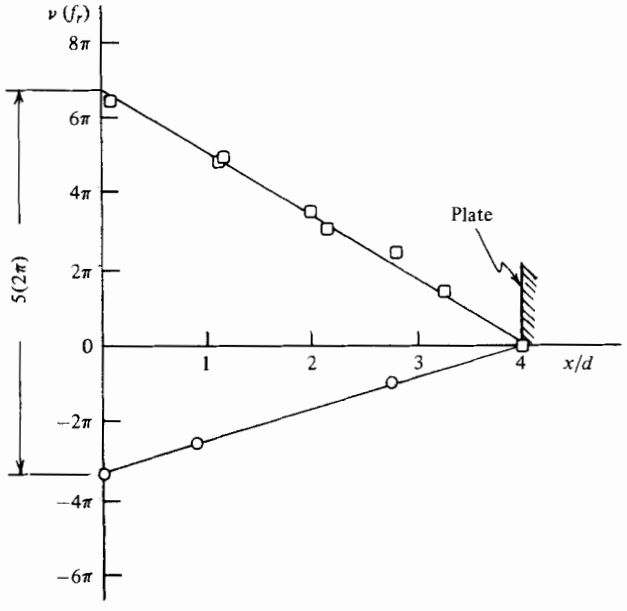

FIGURE 13. Phase-difference variations of the two waves at the resonant frequency ($M = 0{\cdot}8$, $x_0/d = 4$, $f_r = 5{\cdot}5$ kHz, $r_r/d = 1$). The downward-sloping line has a slope $\propto$ (large-scale eddy convection velocity)$^{-1}$; the upward-sloping line has slope $\sim$ (speed of sound)$^{-1}$.

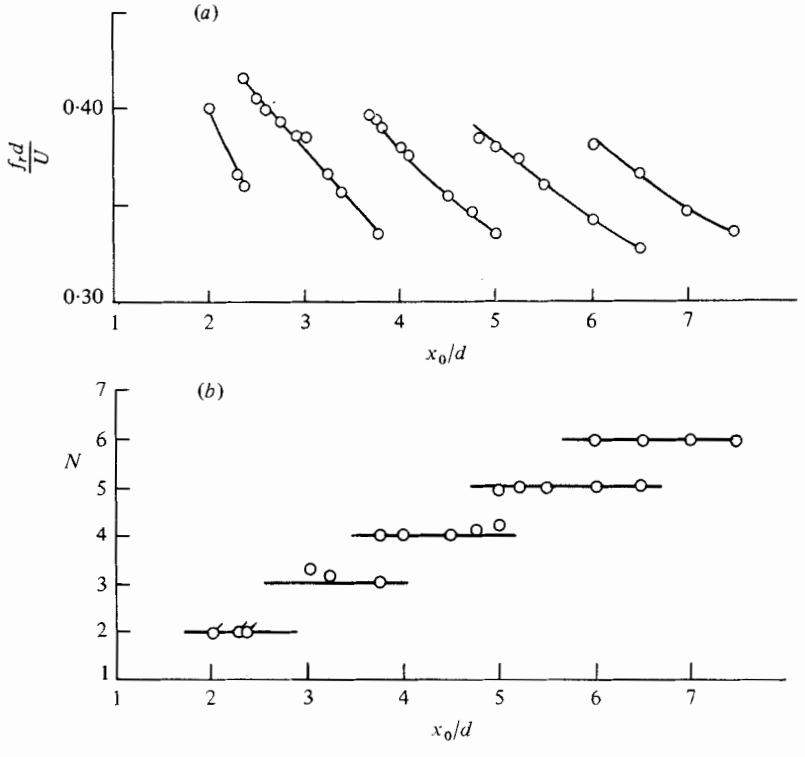

FIGURE 14. (*a*) Variations of the non-dimensional resonant frequency parameter $f_r d/U$ with plate locations, $M = 0{\cdot}9$. (*b*) Resonant frequency stages, $N = x_0/\lambda_1 + x_0/\lambda_2$, ○, measured; ◌, calculated from equation (7*a*) with f_r measured from a surface pressure transducer and $C_1/U = 0{\cdot}62$.

Frequency stage N	x_0/d From equation (7b)	x_0/d Measured
1	1·25	—
2	2·50	2·40
3	3·74	3·75
4	4·99	4·8–5·0
5	6·24	6·0–6·5
6	7·49	7·50

TABLE 1. Relative distance between nozzle exit and plate at frequency discontinuities. (M = 0·9, θ_a = 25°, K_v = 0·62.)

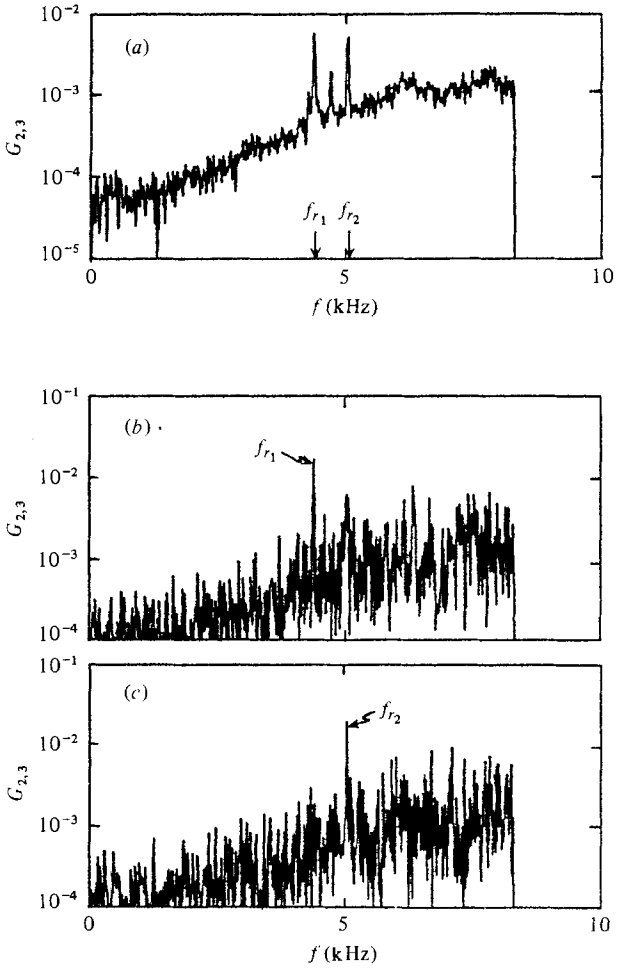

FIGURE 15. The frequency jump phenomenon (M = 0·9, x_0/d = 2·35). (*a*) Long-time-averaged (2·4 s) cross-spectrum. (*b*) and (*c*) Two short-time-averaged (0·061 s) cross-spectra.

decreased until a minimum value is attained. A further increase in the nozzle-to-plate distance results in a frequency jump to a higher value and the number of waves in the feedback loop is increased by one.

The lower limit of the resonant frequency at the discontinuity between frequency stages was found to be $St \simeq 0{\cdot}33$. Significantly, this value corresponds closely to the most unstable mode of a free jet column measured by Crow & Champagne (1971) for an incompressible flow condition. The lower limit of the resonant frequency and the limitation to integer wavenumbers in the feedback loop (equation (7*a*)) can be used to predict the positions of the plate at which discontinuities between frequency stages occur. Equation (7*a*) is rewritten in the form

$$\frac{x_0}{d} = \frac{1}{(St)_r} \frac{N}{1/K_v + M\cos\theta_a}, \tag{7b}$$

where $(St)_r = (St)_{\min} = 0{\cdot}33$ and $Kv = C_1/U$. A comparison between the locations of the plate at which frequency discontinuities occur as predicted by equation (7*a*) and as measured is presented in table 1. The predicted values in the second column are in good agreement with the measured values in the third column.

Hysteresis is also observed. For example, there are two resonant frequencies at $x_0/d = 2{\cdot}35$ (figure 15). The long-time-averaged cross-spectrum between two surface pressure signals shows two peaks. When the spectrum of the same signal is calculated over short time intervals, often only a single peak appears. It indicates that the flow switches from one resonant mode to another mode intermittently at the frequency discontinuities.

3.3. *The collective interaction*

It has been proved that the upstream-propagating waves force the flow near the nozzle exit. It is then logical to examine the response of the intrinsically unstable shear layer to such a forcing. The raw pressure signal very close to the nozzle ($x/d = 0{\cdot}13$) clearly shows (figure 16) high-frequency fluctuations superimposed on low ones. The spectrum of the signal is plotted in figure 17. A broadband high-frequency peak appears besides the dominant resonant frequency peak. The high-frequencies have been measured for different Mach numbers and the Strouhal numbers found to be in the range $3 < St < 5$ and to vary with the square root of the Mach number (figure 18). This result agrees with the theoretical prediction of initial instability frequencies (Michalke 1971). Hence, the high-frequency signals are the instability waves. The initial instability frequencies are measured for both the free jet and the impinging jet (figure 18). The presence of a plate does not change the initial instability frequencies. The resonant frequencies for $M = 0{\cdot}8$ and for $M = 0{\cdot}9$ are also plotted in the same figure. The vertical bars do not represent the range of accuracy of the measurements, but indicate the frequency variations with different plate locations. The resonant frequencies are more than one order of magnitude lower than the instability frequencies.

Farther downstream ($x/d = 1{\cdot}31$), the pressure signal contains predominantly low-frequency fluctuations. In a very short distance, the shear flow changes its characteristic frequency from the high initial instability frequency to the low resonant frequency, which is about ten times lower than the instability frequency. A pairing process, first observed by Winant & Browand (1974) in a two-dimensional shear layer, is not a likely mechanism to produce this frequency reduction: it would take three to four pairings to decrease the frequency by a factor of 10, requiring a long distance not

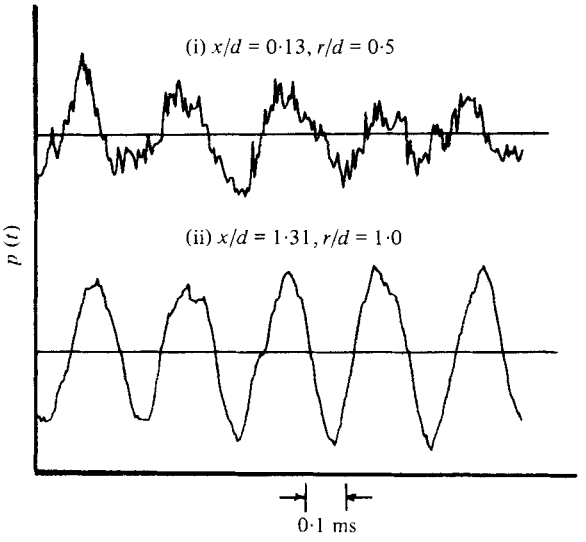

FIGURE 16. Near-field pressure signals in an impinging jet operated in resonance ($M = 0{\cdot}9$, $x_0/d = 4{\cdot}5$). (i) $x/d = 0{\cdot}13$, $r/d = 0{\cdot}5$. (ii) $x/d = 1{\cdot}31$, $r/d = 1{\cdot}0$.

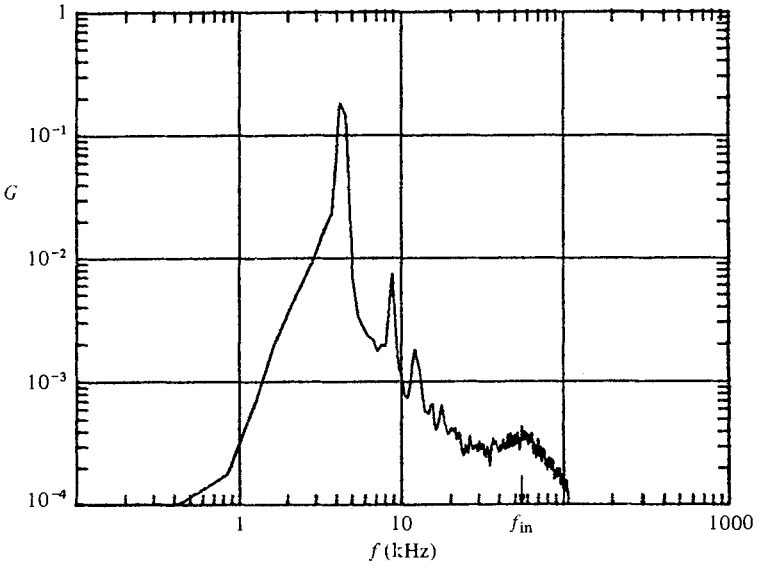

FIGURE 17. Near-field power spectrum for a microphone at $x/d = 0{\cdot}13$ and $r/d = 0{\cdot}5$ ($M = 0{\cdot}9$, $x_0/d = 4{\cdot}5$).

available in this case. In addition, a phase lock between the instability waves and the upstream-propagating waves is not expected because their frequencies are as much as one order of magnitude apart. Therefore, one must search for a new mechanism governing the instability process near the nozzle of a resonant impinging jet.

In a forced plane shear layer, Ho & Huang (1978, 1980) were able to cause a specific number of vortices to merge together by forcing the layer with a certain subharmonic of the self-excited instability frequency. Their work included the case of the forcing frequency being one order of magnitude lower than the initial instability

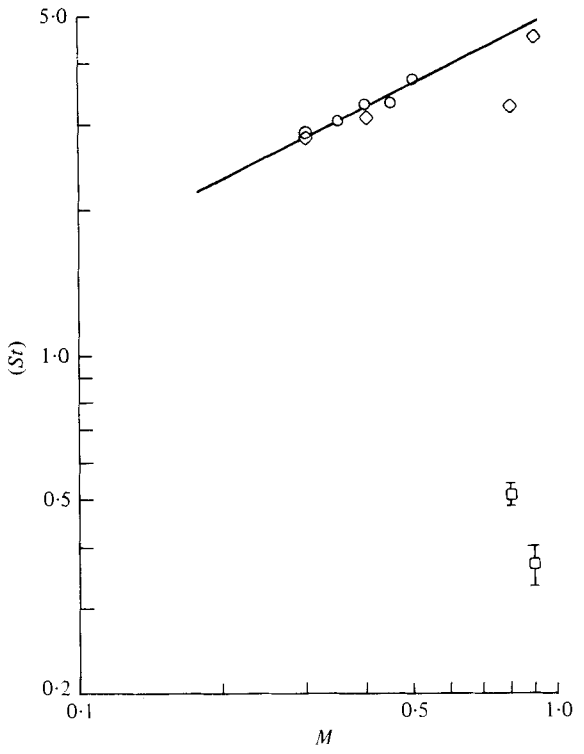

FIGURE 18. Instability and resonant Strouhal numbers for free and impinging jets. ○, $(St)_{in}$, free jet; ◇, $(St)_{in}$, impinging jet; □, $(St)_r$, impinging jet. The straight line has slope $\frac{1}{2}$.

frequency. This is similar to the situation in the present experiment. A photograph of the forced plane shear layer is shown in figure 19. The flow is from left to right with the higher-velocity flow at the lower side. The low-frequency forcing forms a wavy shear layer and displaces the vortices from their original positions. This causes a redistribution of the vortices owing to their induced field (Batchelor 1967). In one part of a period of the wavy shear layer the vortices are drawn together, develop a stronger induced field that causes their rotation around each other and their coalescence into a large vortex. In the other part they are drawn apart, stretch and do not interact. The phenomenon of multiple merging of coherent structures is termed *collective interaction*; it is the mechanism governing the stability process near the nozzle of the impinging jet. Two of the characteristic features associated with the collective interaction are a sharp drop in passage frequency and a relatively large shear-layer growth. The idea of the collective interaction could explain the relative large growth rate of a forced two-dimensional shear layer observed by Wygnanski, Oster & Fiedler (1979).

The schematic drawing in figure 20 describes the collective interaction in an impinging jet. The shear layer emerging from the nozzle is flapping due to the periodic forcing from the upstream-travelling waves. The shear layer goes through cycles of divergence ($t = 0, T_r, 2T_r, \ldots$) and convergence ($t = T_r/2, 3T_r/2, \ldots$), where T_r is the period of the resonant frequency. At $t = 0$, the small vortices rotate around each other under their induced field and coalesce into a large vortical structure. At $t = T_r/2$, the shear layer

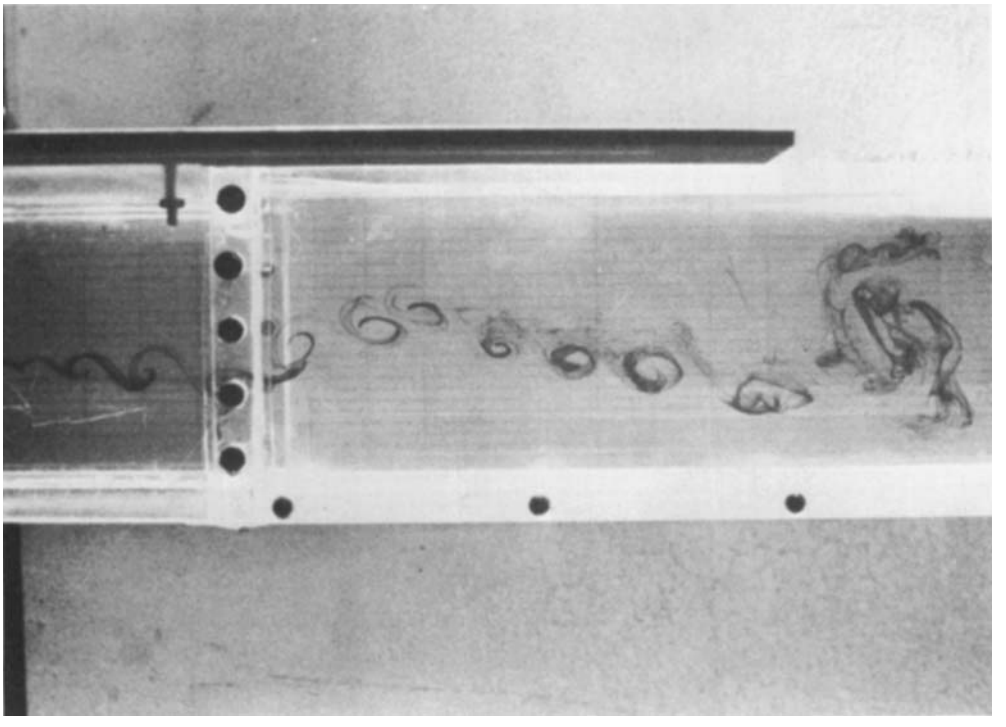

FIGURE 19. Collective interaction in a two-dimensional free shear layer, flow from left to right, forcing frequency $\ll$ natural initial instability frequency (Ho & Huang 1978).

changes its orientation and the lower vortices move away from the upper vortices due to the mean shear. Therefore, this portion of the shear layer tends to stretch. The vortices are stable, and do not coalesce. These sketches show the evolution of the merging of multiple vortices under forcing. Apparently the passage frequency can drop by one order of magnitude within a short distance. Nosseir & Ho (1980) separated portions of the measured pressure fluctuations induced by the passage of the large coherent vortices and those portions induced by the passage of the 'valley' between two vortices. Their spectral analysis of the separated portions, using the maximum entropy method, confirmed the multiple merging of small-scale vortices into a large coherent vortex in agreement with the collective interaction concept described earlier. It should be pointed out here that the collective interaction is a nonlinear secondary instability. In the plane shear-layer experiment (Ho & Huang 1978, 1980), high-amplitude forcing is necessary if the forcing frequency is one order of magnitude lower than the initial instability frequency. In the impinging jet, the collective interaction becomes predominant at high Mach numbers, since the amplitude of the upstream acoustic forcing waves increases rapidly with the Mach number. The reason for requiring high-amplitude forcing is the very slow growth rate of the low-frequency waves in the thin shear layer according to the linear theory (Michalke 1971). Only high-amplitude nonlinear forcing can make this phenomenon occur in a short distance from the nozzle. Owing to the collective interaction, the high-frequency initial instability waves do not play an important role in the flow with self-sustained oscillations.

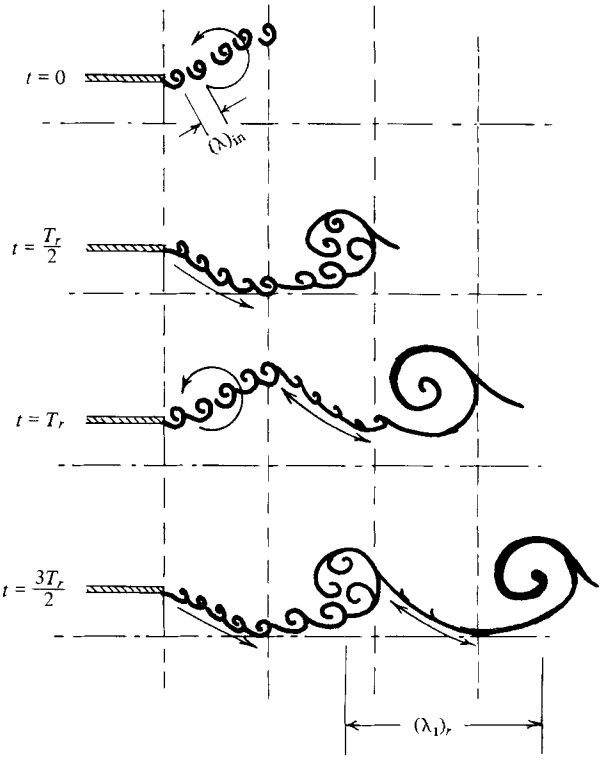

FIGURE 20. Collective interaction.

The low-frequency long waves travelling downstream and upstream are much more important.

After the collective interaction the passage frequency remains constant downstream to the plate. It implies that the coherent structures do not merge again. In the experiment by Ho & Huang (1978, 1980), a high-amplitude subharmonic is needed for the coherent structures to merge. A long distance and a thick shear layer are required for the growth of the subharmonic. In an impinging jet neither of these requirements are met for the subharmonics. Hence, no further merging appears after the collective interaction, and the passage frequency of the coherent structures after the collective interaction becomes the dominant resonant frequency.

4. Conclusions

The present study has established experimental evidence of a feedback mechanism and an instability process, the collective interaction, essential to the onset of resonance in an impinging jet. The feedback loop (figure 21) is formed by the downstream-convected large coherent structures and by upstream-propagating pressure waves generated by the impingement of these structures on the plate. The upstream-propagating waves travel with the speed of sound in the quiescent medium. These waves force in-phase oscillations of the thin shear layer near the nozzle exit. The shear layer, oscillating at a frequency much lower than its intrinsic most unstable frequency,

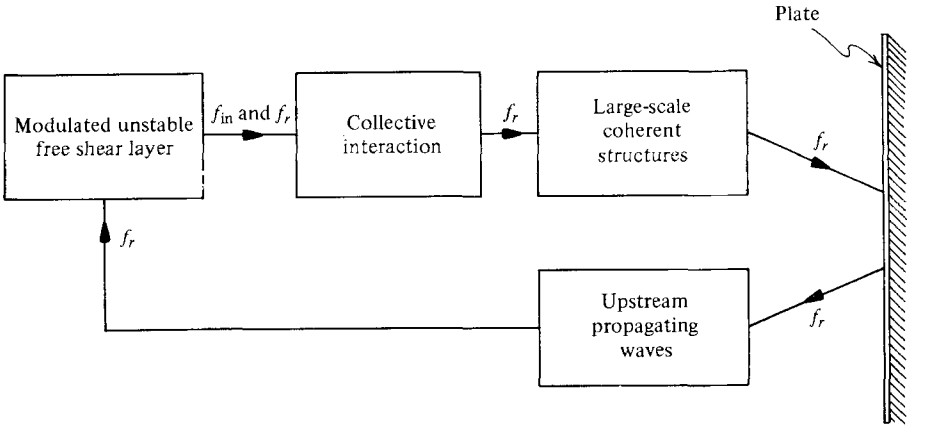

FIGURE 21. Schematic diagram of the feedback loop in an impinging jet.

undergoes a collective interaction in which many small vortices merge together to form a large coherent structure. The collective interaction, therefore, generates large coherent structures at intervals phase-locked with the external forcing of the upstream-propagating waves causing the resonance. The sharp drop in the passage frequency of the vortices concurrent with the rapid growth of the shear layer within a short distance from the nozzle, by the collective interaction, makes the resonance independent of the initial conditions of the jet.

We would like to thank Dr J. Laufer for his helpful discussions. This work is sponsored by AFOSR under Grant 77-3312 and contract F49620-78-C-0060.

Appendix

The following is a simple mathematical model to explain the characteristics of measured correlation functions in the impinging jet with two counter-propagating waves. The pressure at any point with a position vector ξ in the near field is the superposition of two waves and takes the form

$$p(t,\xi) = a(\xi)\exp i(\omega_r t - \mathbf{K}_1 x + \nu_c) + b(\xi)\exp i(\omega_r t + \mathbf{K}_2.\xi), \tag{8}$$

where the two waves are assumed to be monochromatic plane waves having the same frequency f_r which is the resonant frequency. The wavenumbers, $\mathbf{K}_1$ and $\mathbf{K}_2$, are different, however, because of different phase velocities. The first term in (8) represents a downstream-travelling pressure wave due to the large-scale structures and having a velocity $C_1 = \omega_r/|\mathbf{K}_1|$. The second term is an upstream wave travelling in θ_a direction with velocity

$$\mathbf{C}_2 = \frac{\omega_r}{|\mathbf{K}_2|}\boldsymbol{\theta}_a.$$

The phase difference between the two waves at any location is

$$\nu = -\mathbf{K}_1 x - \mathbf{K}_2.\xi + \nu_c, \tag{9}$$

where the constant phase shift ν_c can be evaluated by applying the boundary condition at the plate. Since the upstream-propagating wave is assumed to be generated by the

downstream-travelling wave as it impinges on the plate, the phase difference between the two waves should be equal to zero there, i.e.

$$\nu = 0 \quad \text{at} \quad \boldsymbol{\xi} = \boldsymbol{\xi}_s,$$

where $\boldsymbol{\xi}_s$ is the position vector of an apparent sound source on the plate. Substituting in (9), one obtains

$$\nu_c = |\mathbf{K}_1| x_0 + \mathbf{K}_2 . \boldsymbol{\xi}_s, \quad \nu = |\mathbf{K}_1| (x - x_0) + \mathbf{K}_2 . (\boldsymbol{\xi}_s - \boldsymbol{\xi}). \tag{10}$$

The pressure in (8) can be written in the simple form

$$p(t, \boldsymbol{\xi}) = A\alpha + B\beta,$$

where the coefficients A and B are functions of the position and represent the amplitudes of the two waves α and β.

The correlation between pressure signals at the points x_i and x_j in the near field is

$$R_{i,j}(\tau) = \lim_{T \to \infty} \frac{1}{T} \int_0^T p(t, \boldsymbol{\xi}_i)\, p(t+\tau, \boldsymbol{\xi}_j) d\tau.$$

Substituting from (11), one gets

$$R_{i,j}(\tau) = A_i A_j R_{\alpha_i, \alpha_j}(\tau) + B_i B_j R_{\beta_i, \beta_j}(\tau) + A_i B_j R_{\alpha_i, \beta_j}(\tau) + A_j B_i R_{\beta_i, \alpha_j}(\tau). \tag{11}$$

The above equation shows that the correlation $R_{i,j}(\tau)$ of two signals, each of which is the sum of two stationary components, is the algebraic sum of the individual component correlations. The correlations of these components give the four correlation time delays in (5) according to the following sequence:

$$\begin{aligned}
R_{\alpha_i, \alpha_j}(\tau) &\to \tau^{[1]} = (x_j - x_i)/C_1, \\
R_{\beta_i, \beta_j}(\tau) &\to \tau^{[2]} = -\boldsymbol{\xi}_{i,j} . \boldsymbol{\theta}_a / C_2, \\
R_{\alpha_i, \beta_j}(\tau) &\to \tau^{[3]} = -\left(\frac{x_0 - x_j}{C_1} + \frac{\boldsymbol{\xi}_{i,s} . \boldsymbol{\theta}_a}{C_2} \right), \\
R_{\beta_i, \alpha_j}(\tau) &\to \tau^{[4]} = \left(\frac{x_0 - x_i}{C_1} + \frac{\boldsymbol{\xi}_{j,s} . \boldsymbol{\theta}_a}{C_2} \right).
\end{aligned}$$

REFERENCES

Batchelor, G. K. 1967 *An Introduction to Fluid Dynamics*, pp. 511–517. Cambridge University Press.

Browand, F. K. & Laufer, J. 1975 The role of large scale structures in the initial development of circular jet. *Proc. 4th Biennial Symp. Turbulence in Liquids, Univ. Missouri-Rolla*, pp. 333–344. Princeton, New Jersey: Science.

Brown, G. & Roshko, A. 1971 The effect of density difference on the turbulent mixing layer. *AGARD Conf. Proc.* no. 93, paper 23.

Crow, S. C. & Champagne, F. H. 1971 Orderly structure in jet turbulence. *J. Fluid Mech.* **48**, 547–591.

Donaldson, C., Snedeker, R. S. & Margolis, D. P. 1971 A study of free jet impingement. Part 2. Free jet turbulent structure and impingement heat transfer. *J. Fluid Mech.* **45**, 477–512.

Foss, J. F. & Kleis, S. J. 1976 Mean flow characteristics for the oblique impingement of an axisymmetric jet. *A.I.A.A. J.* **14**, 705–706.

GUTMARK, E., WOLFSHTEIN, M. & WYGNANSKI, I. 1978 The plane turbulent impinging jet. *J. Fluid Mech.* **88**, 737–756.

HO, C. M. & HUANG, L. S. 1978 Subharmonics and vortex merging in an unsteady shear layer. *Bull. Am. Phys. Soc.* **23**, 1007.

HO, C. M. & HUANG, L. S. 1980 Subharmonics and vortex merging in mixing layers. *J. Fluid Mech.* (submitted).

HO, C. M. & NOSSEIR, N. S. 1980 Large coherent structures in an impinging turbulent jet. *Turbulent Shear Flows* 2, p. 297. Springer.

HO, C. M., PLOCHER, D. A. & LEVE, H. L. 1977 Surface pressure fluctuations generated by a jet impinging on a curved plate. *A.I.A.A. paper* no. 77–114.

KOVASZNAY, L. S. G., KIBENS, V. & BLACKWELDER, R. F. 1970 Large-scale motion in the intermittent region of a turbulent boundary layer. *J. Fluid Mech.* **41**, 283–325.

LAU, J. C., FISHER, M. J. & FUCHS, H. V. 1972 The intrinsic structure of turbulent jets. *J. Sound Vib.* **22**, 379–406.

MICHALKE, A. 1972 Instabilität eines kompressiblen runden Freistrahls unter Berücksichtigung des Einflusses der Strahlgrenzschichtdicke. *Z. Flugwiss.* **19**, 319–328.

NEUWERTH, G. 1973 Dr.-Ing. Thesis. Tech. Hochsch. Aachen, West Germany.

NOSSEIR, N. S. 1979 On the feedback phenomenon and noise generation of an impinging jet. Ph.D. thesis, Univ. of Southern Calif., U.S.A.

NOSSEIR, N. S. & HO, C. M. 1980 Pressure fields generated by instability waves and coherent structures in an impinging jet. *A.I.A.A. paper no.* 80–0980.

POWELL, A. 1961 On the edgetone. *J. Acoust. Soc. Am.* **33**, 395–409.

RIBNER, H. S. 1957 Reflection, transmission, and amplification of sound by a moving medium. *J. Acoust. Soc. Am.* **29**, 435–441.

ROCKWELL, D. & NAUDASCHER, E. 1979 Self-sustained oscillations of impinging free shear layer. *Ann. Rev. Fluid Mech.* **11**, 67–94.

TAM, C. & BLOCK, P. J. W. 1978 On the tones and pressure oscillations induced by flow over rectangular cavities. *J. Fluid Mech.* **89**, 373–399.

TOWNSEND, A. A. 1956 The structure of turbulent shear flow. Cambridge University Press.

WAGNER, F. R. 1971 The sound and flow field of an axially symmetric free jet upon impact on a wall. *N.A.S.A.* TT F-13942.

WILLIAMS, K. C. & PURDY, K. R. 1970 A prewhitening technique for recording acoustic turbulent flow data. *Rev. Sci. Instrum.* **41**, 1897–1899.

WINANT, C. D. & BROWAND, F. K. 1974 Vortex pairing: the mechanism of turbulent mixing layer growth at moderate Reynolds number. *J. Fluid Mech.* **63**, 237–255.

WYGNANSKI, I., OSTER, D. & FIEDLER, H. 1979 The forced, plane, turbulent mixing-layer: a challenge for the predictor. *Proc. 2nd Int. Symp. Turbulent Shear Flows, London*, 8.12–8.17. Springer.